SUPPORTING INFORMATION

Less Active CeO_2 regulating Bifunctional Oxygen Electrocatalytic Activity of Co_3O_4@N-doped Carbon for Zn-air Battery

Xiaobo He[1, 3]┼, Xuerui Yi[2]┼, Fengxiang Yin[1, 3], Biaohua Chen[1], Guoru Li[1], Huaqiang Yin[4]*

[1] *Jiangsu Key Laboratory of Advanced Catalytic Materials and Technology, School of Petrochemical Engineering, Changzhou University, Changzhou 213164, China*

[2] *College of Chemical Engineering, Beijing University of Chemical Technology, Beijing 100029, PR China*

[3] *Changzhou Institute of Advanced Materials, Beijing University of Chemical Technology, Changzhou 213164, PR China*

[4] *Key Laboratory of Advanced Reactor Engineering and Safety, Ministry of Education, Tsinghua University, Beijing 100084, PR China*

**Corresponding author*

Tel.: +86-519-86330253

E-mail: yinfx@cczu.edu.cn (F. Yin)

┼ *These authors contributed equally.*

RHE conversion

We have calibrated the reference electrode to RHE by the method presented in Y.Y. Liang, et al. (Nature Mater. 2011, 10, 780-786.). The calibration was conducted in a H_2-saturated 0.1 M KOH electrolyte with a Pt wire as the working electrode. The CV was run at a sweep rate of 1 mV s^{-1} and the average of two potentials at which current crossed zero was regarded as the thermodynamic potential of hydrogen electrode reaction.

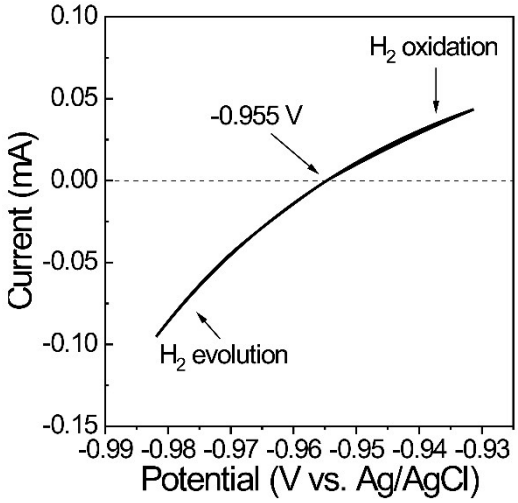

In this study, the potentials measured have been calibrated by the following equation: $E_{(RHE)}=E_{(Ag/AgCl)}+0.955$ V.

Supplementary Figures and Notes

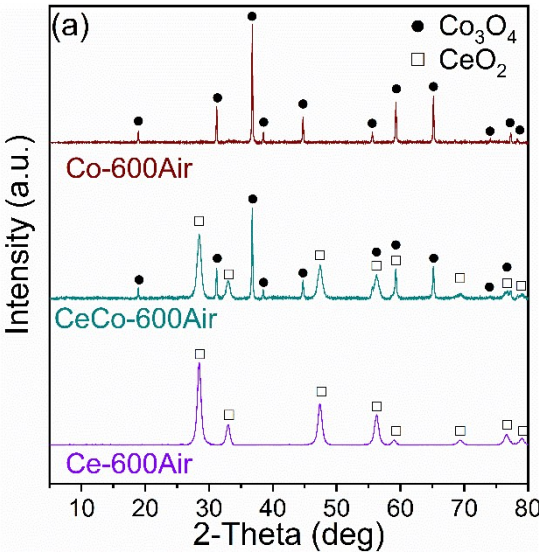

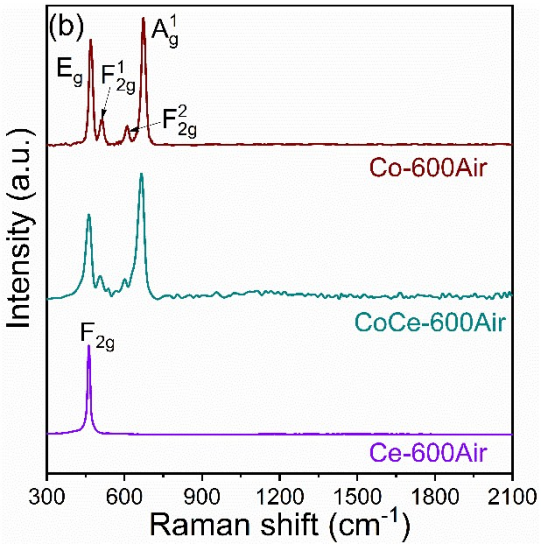

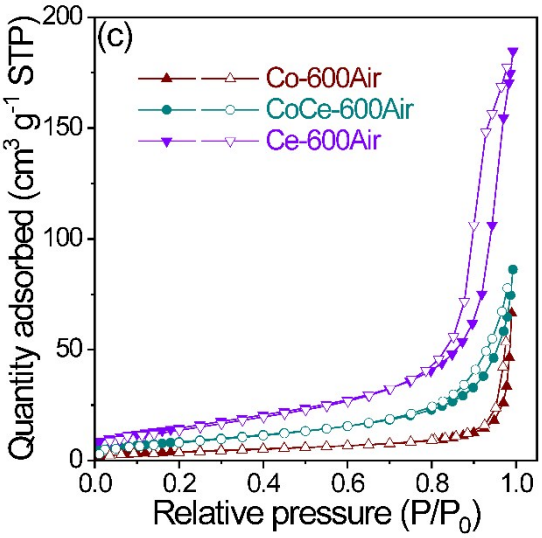

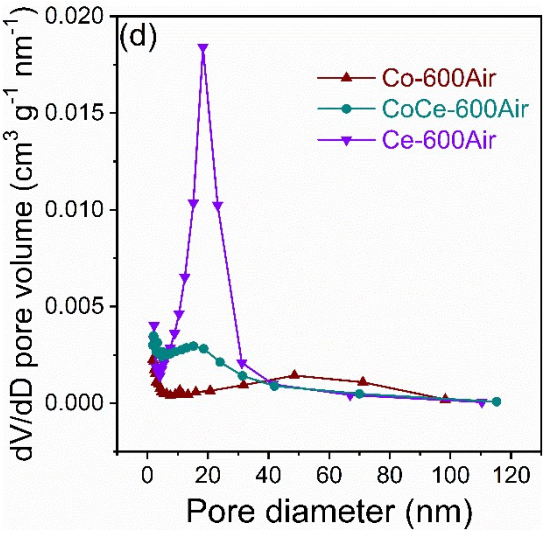

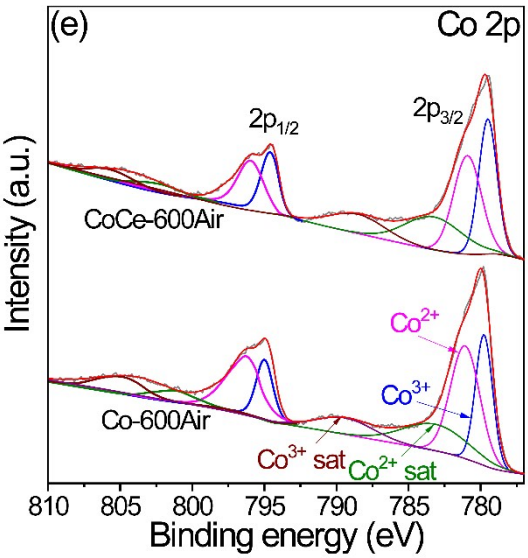

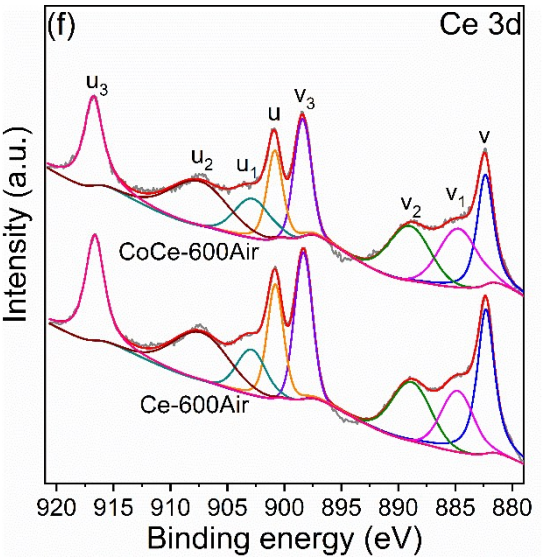

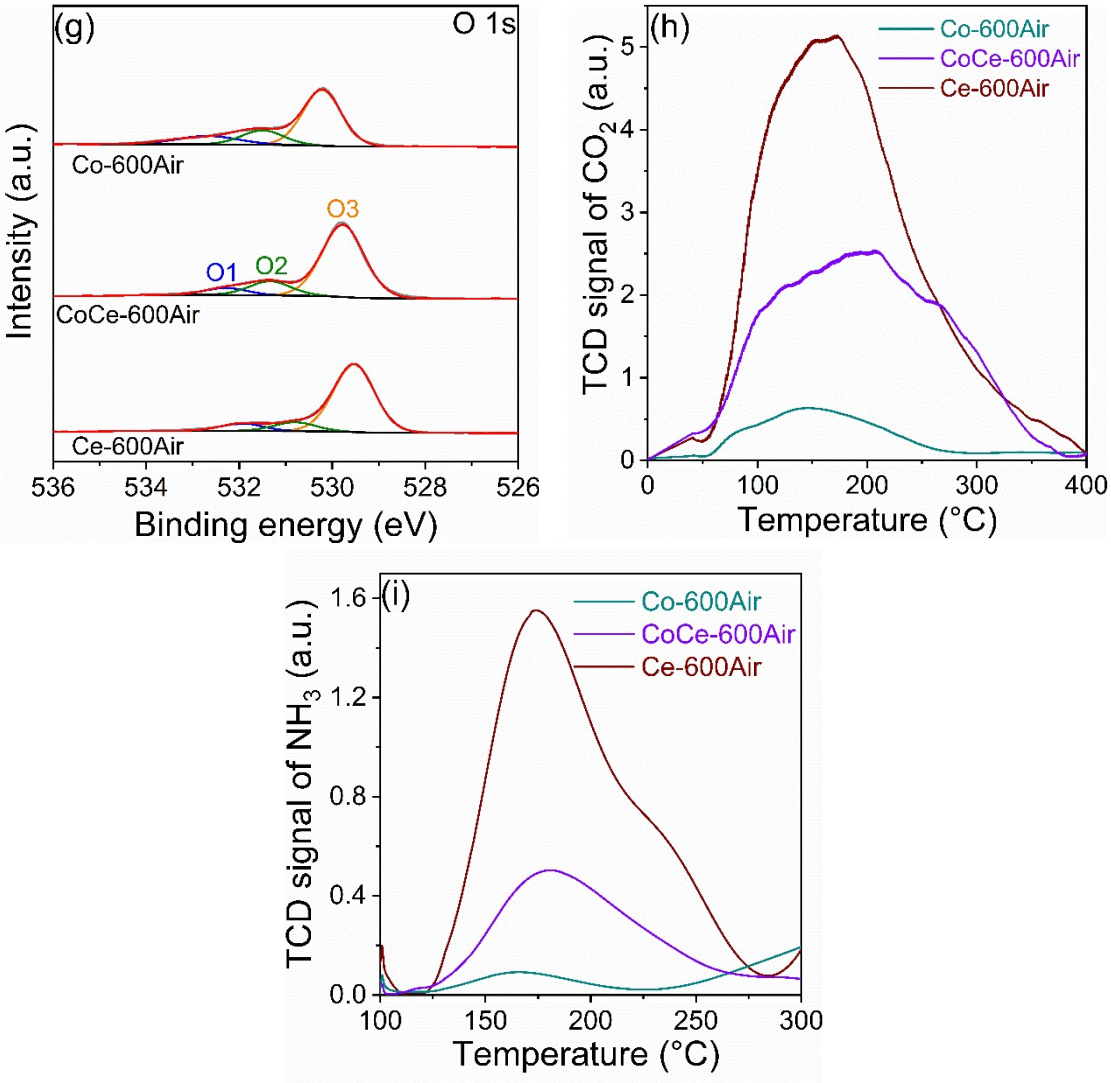

Fig. S1. Structural information of the samples prepared in air, including Co-600Air, CoCe-600Air, and Ce-600Air: (a) XRD patterns, (b) Raman spectra, (c) N_2 adsorption-desorption isotherms, (d) Pore size distributions, (e) XPS spectra of Co 2p, (f) XPS spectra of Ce 3d, (g) XPS spectra of O 1s, (h) CO_2-TPD curves, and (i) NH_3-TPD curves.

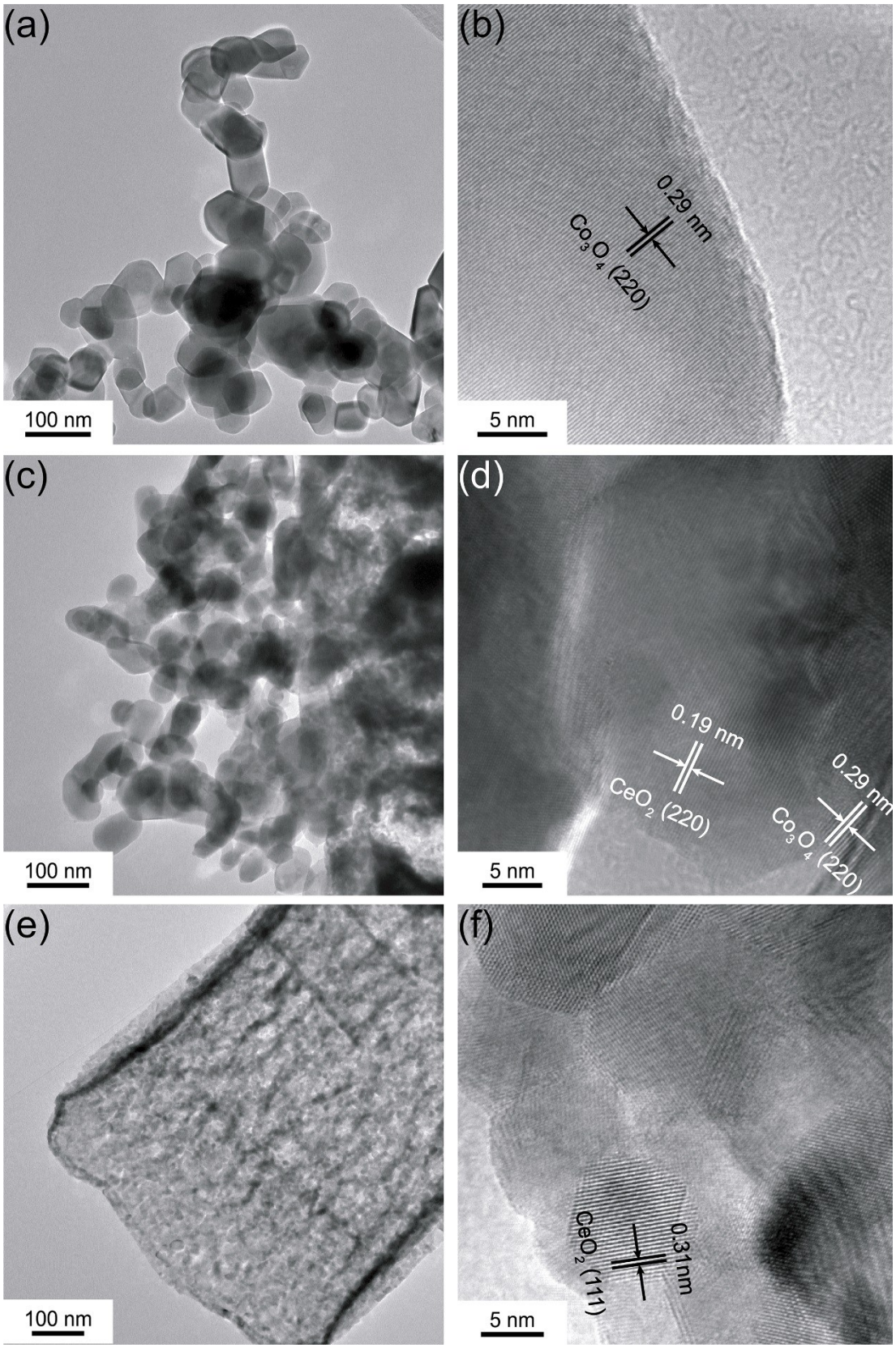

Fig. S2. TEM and HRTEM images: (a) and (b) Co-600Air; (c) and (d) CoCe-600Air; (e) and (f) Ce-600Air.

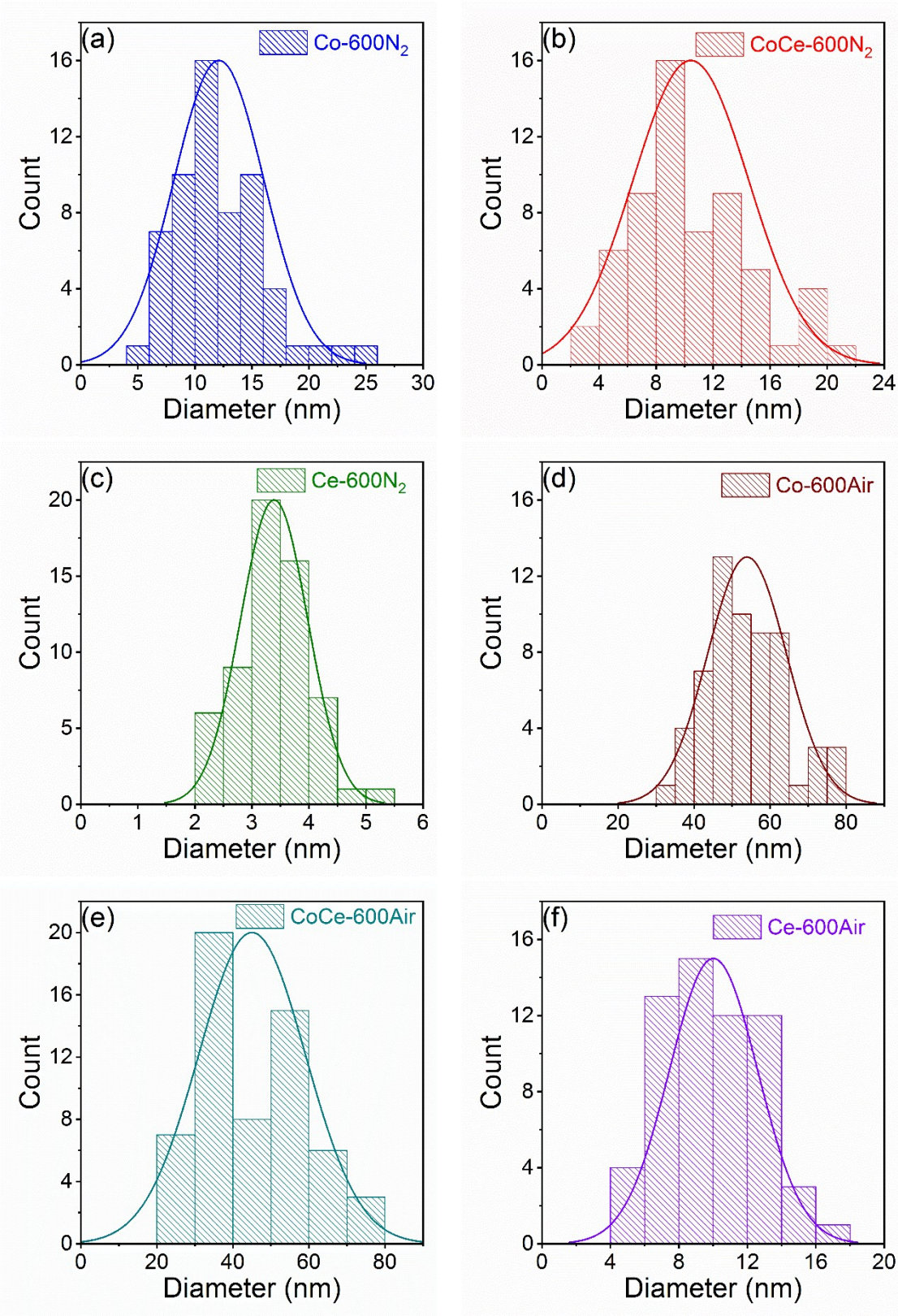

Fig. S3. Size distribution of nanoparticles of the resulting electrocatalysts. (a) Co-600N_2. (b) CoCe-600N_2. (c) Ce-600N_2. (d) Co-600Air. (e) CoCe-600Air (f) Ce-600Air.

Note S1. Structural characterizations of the samples prepared in air, including Co-600Air, CoCe-600Air and Ce-600Air.

Fig. S1a shows the XRD patterns of Co-600Air, CoCe-600Air and Ce-600Air. The diffraction peaks show that Co-600Air and Ce-600Air contain Co_3O_4 ($PDF_2$65-3103) and CeO_2 ($PDF_2$34-0394), respectively. The CoCe-600Air includes both Co_3O_4 and CeO_2. Fig. S1b show the Raman spectra of the samples prepared in air. Both Co-600Air and CoCe-600Air show four distinct peaks at 466 cm^{-1}, ~510 cm^{-1}, ~608 cm^{-1} and ~670 cm^{-1} correspond to the E_g, F_{2g}^1, F_{2g}^2 and A_g^1 bands for Co_3O_4, respectively. Ce-600Air shows the single F_{2g} peak for CeO_2 at 464 cm^{-1}. Notably, the peak around 466 cm^{-1} in CoCe-600Air can be assigned to the combined contributions from the F_{2g} for CeO_2 and the E_g for Co_3O_4. The N_2 adsorption-desorption isotherms of Co-600Air, CoCe-600Air and Ce-600Air are shown in Fig. S1c. The solid and hollow marks represent the adsorption and desorption branches, respectively. The typical H3-typed hysteresis loops were observed, suggesting mesopores in these electrocatalysts. Fig. S1d shows the pore size distributions of the samples. The average pore sizes of mesopores are ~2.05 nm, ~2.04 nm and ~2.22 nm for Co-600Air, CoCe-600Air and Ce-600Air, respectively. The BET specific surface areas (SSAs) of Co-600Air, CoCe-600Air and Ce-600Air are ~15.1 m^2 g^{-1}, ~31.5 m^2 g^{-1} and ~54.8 m^2 g^{-1}, respectively. The pore volumes of Co-600Air, CoCe-600Air and Ce-600Air are ~0.03 cm^3 g^{-1}, ~0.07 cm^3 g^{-1} and ~0.18 cm^3 g^{-1}, respectively. The relevant parameters of the pores in them are summarized in Table S1. The Co 2p, Ce3d and O 1s XPS spectra of the samples prepared in air are shown in Fig. S1e-1g and Table S2. The binding energies of Co^{2+}

and Co^{3+} of Co $2p_{3/2}$ in CoCe-600Air have some shifts toward the lower binding energy relative to Co-600Air. The binding energy of Ce species (Ce^{4+} and Ce^{3+}) in CoCe-600Air is slightly shifted toward the higher binding energy. The binding energies of O1, O2 and O3 in CoCe-600Air show some shifts toward the higher binding energy compared to Ce-600Air, but still lower than those in Co-600Air. CO_2-TPD results (Fig. S1h) show the CO_2 desorption peaks of Co-600Air, CoCe-600Air and Ce-600Air centers at ~146.2 ºC, ~206.9 ºC and ~173.4 ºC, respectively. The calculated basicity amounts of Co-600Air, CoCe-600Air and Ce-600Air are ~0.03 mmol g^{-1}, ~0.15 mmol g^{-1} and ~0.25 mmol g^{-1}, respectively. NH_3-TPD results (Fig. S1i) show the NH_3 desorption peaks of Co-600Air, CoCe-600Air and Ce-600Air centers at ~166.3 ºC, ~181.1 ºC and ~174.3 ºC, respectively. The calculated acidity amounts of Co-600Air, CoCe-600Air and Ce-600Air are ~0.04 mmol g^{-1}, ~0.39 mmol g^{-1} and ~1.24 mmol g^{-1}, respectively. Fig. S2 shows the TEM and HRTEM images for Co-600Air, CoCe-600Air and Ce-600Air. The TEM image of Co-600Air (Fig. S2a) exhibits the irregularly shaped nanoparticles. HRTEM image (Fig. S2b) shows the d-spacing value of ~0.29 nm, corresponding to the (220) plane of Co_3O_4. In CoCe-600Air, the CeO_2/Co_3O_4 hybrid nanostructures are observed in its TEM and HRTEM images (Fig. S2c and S2d). The d-spacing of ~0.19 nm and ~0.29 nm are assigned to the (220) plane of the fluorite-typed cubic CeO_2 and the (220) plane of Co_3O_4, respectively. The TEM image of Ce-600Air (Fig. S2e) shows the sheet-like morphology, which is composed of abundant small CeO_2 nanoparticles with non-uniformed sizes (Fig. S3). The HRTEM (Fig. S2f) shows d-spacing of ~0.31 nm, corresponding to the (111) planes of CeO_2.

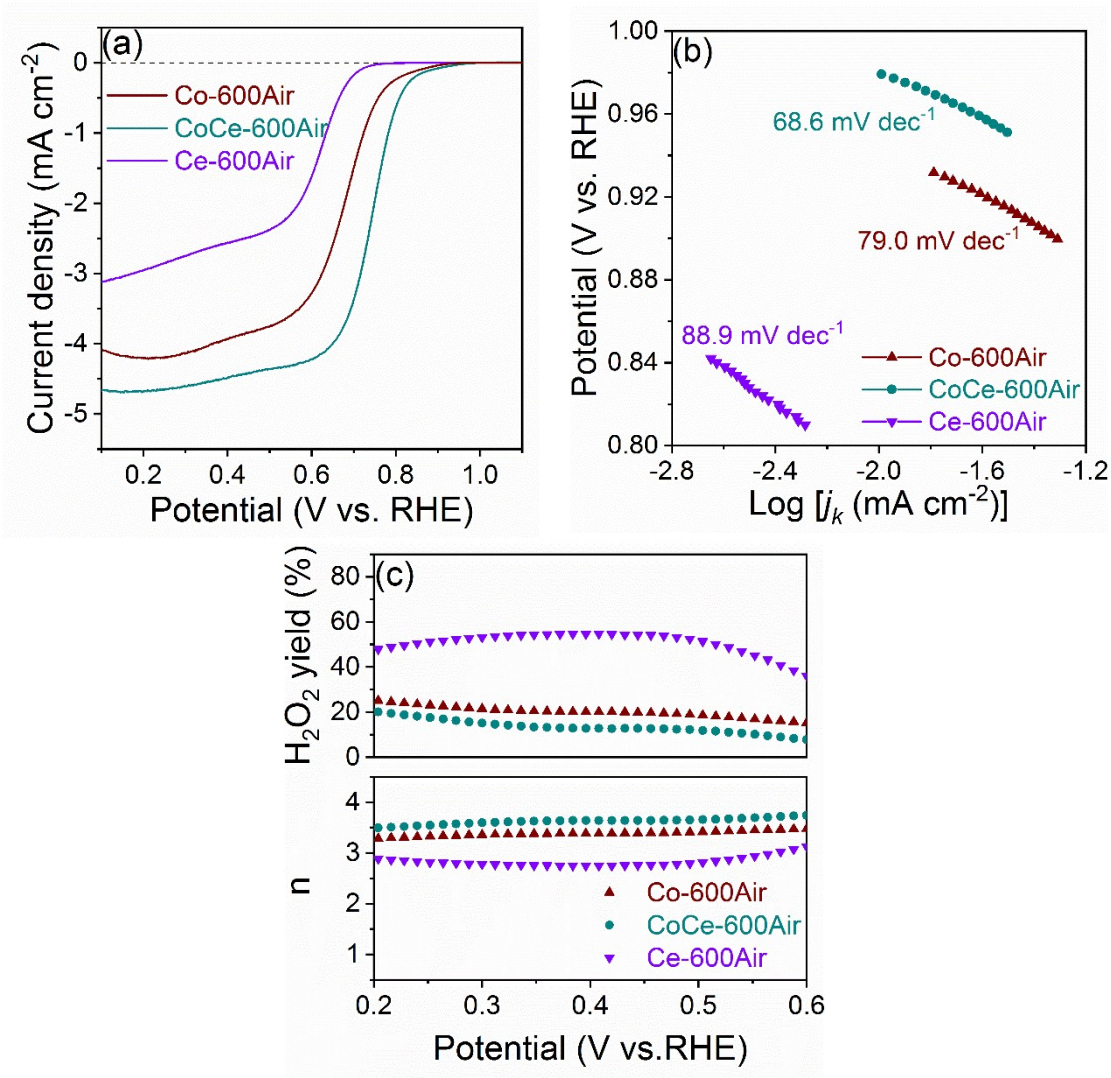

Fig. S4. The ORR and OER activity of Co-600Air, CoCe-600Air, and Ce-600Air: (a) ORR LSV curves at a scan rate of 5 mV s^{-1} under 1600 rpm. (b) The corresponding Tafel plots. (c) The electron transfer number (*n*) and peroxide yield at various potentials.

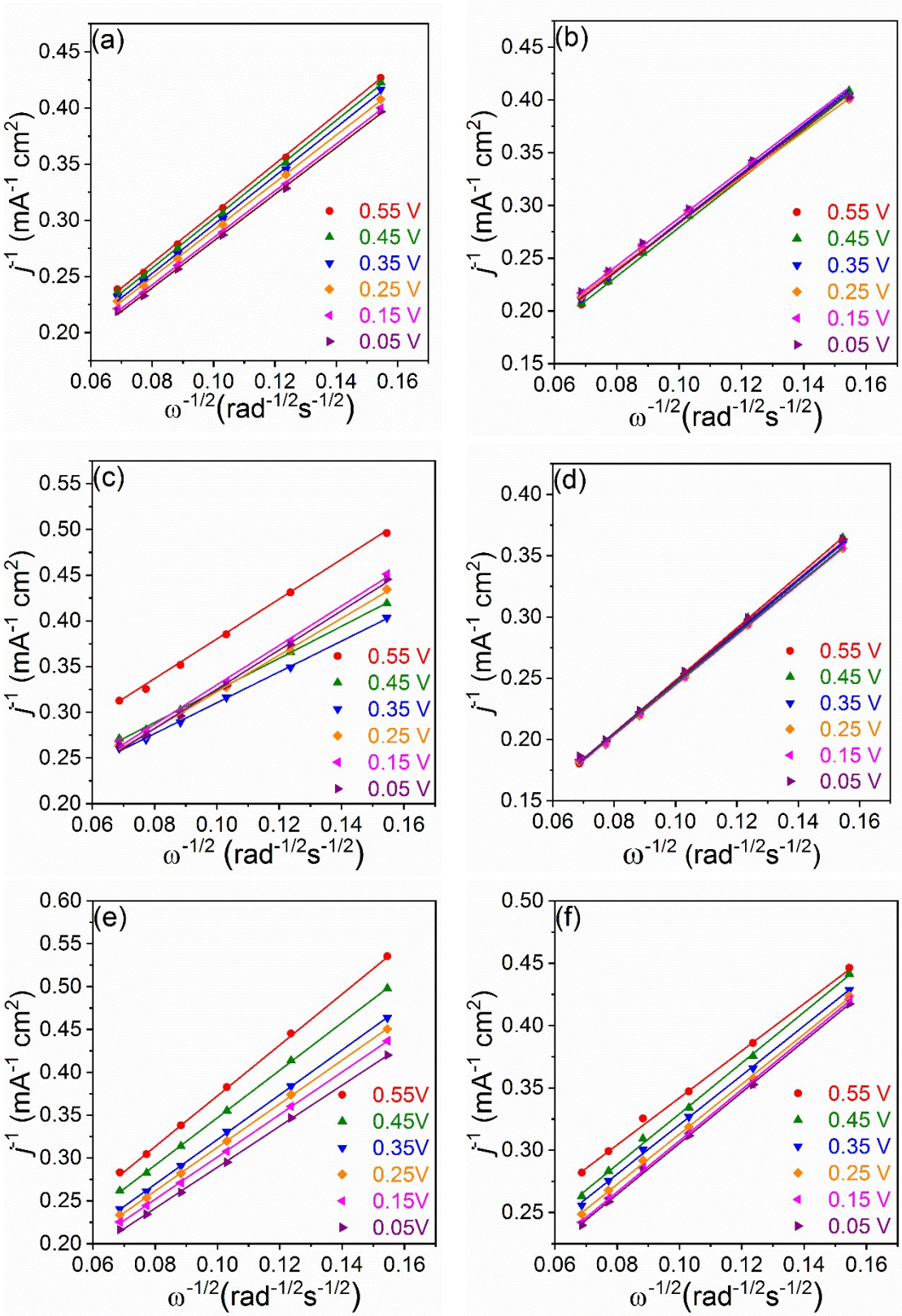
(a)
(b)
(c)
(d)
(e)
(f)
j^{-1} (mA^{-1} cm^2)
$\omega^{-1/2}$(rad$^{-1/2}$s$^{-1/2}$)
0.55 V
0.45 V
0.35 V
0.25 V
0.15 V
0.05 V

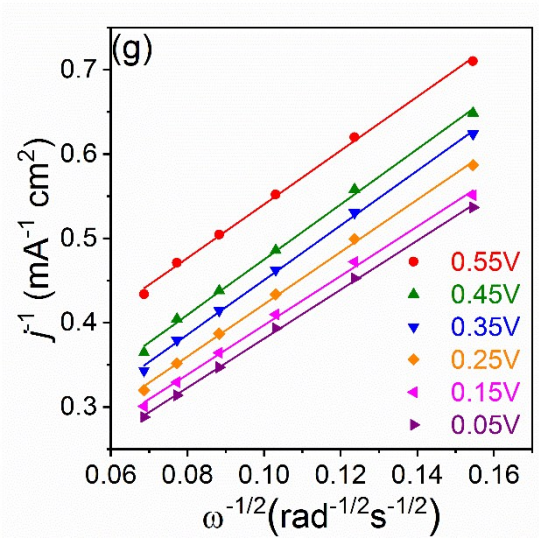

Fig. S5. K-L plots at different potentials of (a) Co-600N_2, (b) CoCe-600N_2, (c) Ce-600N_2, (d) 20 wt% Pt/C, (e) Co-600Air, (f) CeCo-600Air and (g) Ce-600Air.

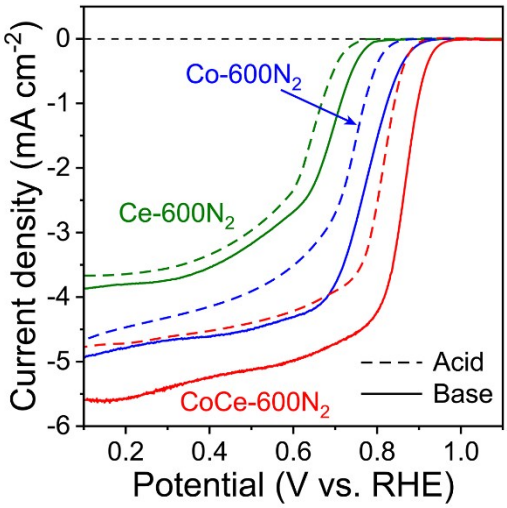

Fig. S6. ORR LSV curves at a scan rate of 5 mV s^{-1} under 1600 rpm in 0.1 M $HClO_4$ (dashed line) and 0.1 M KOH (solid line), respectively, for Co-600N_2, Ce-600N_2 and CeCo-600N_2.

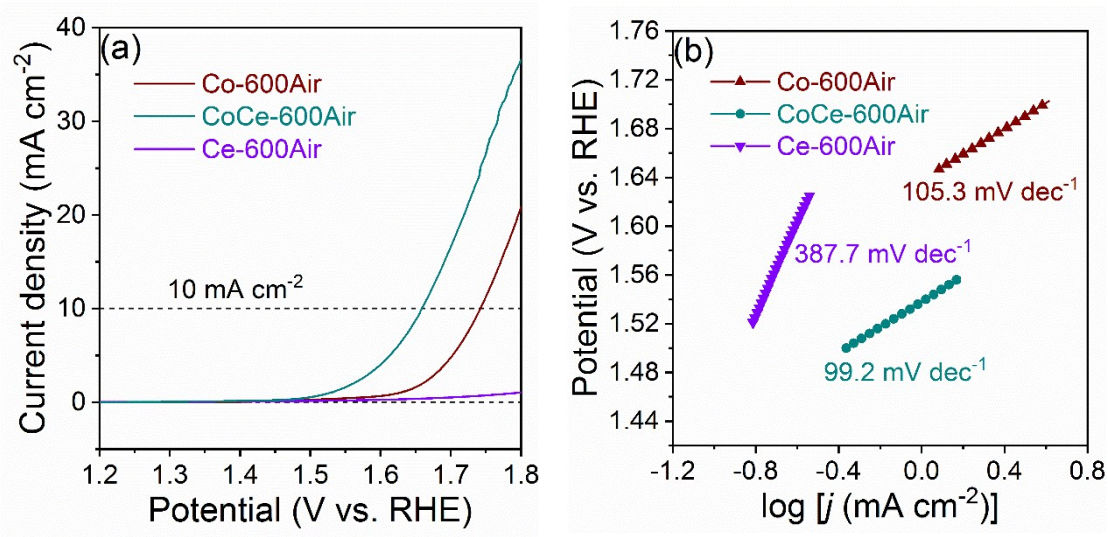

Fig. S7. (a) OER LSV curves at a scan rate of 5 mV s^{-1} under 1600 rpm. (b) The corresponding Tafel plots.

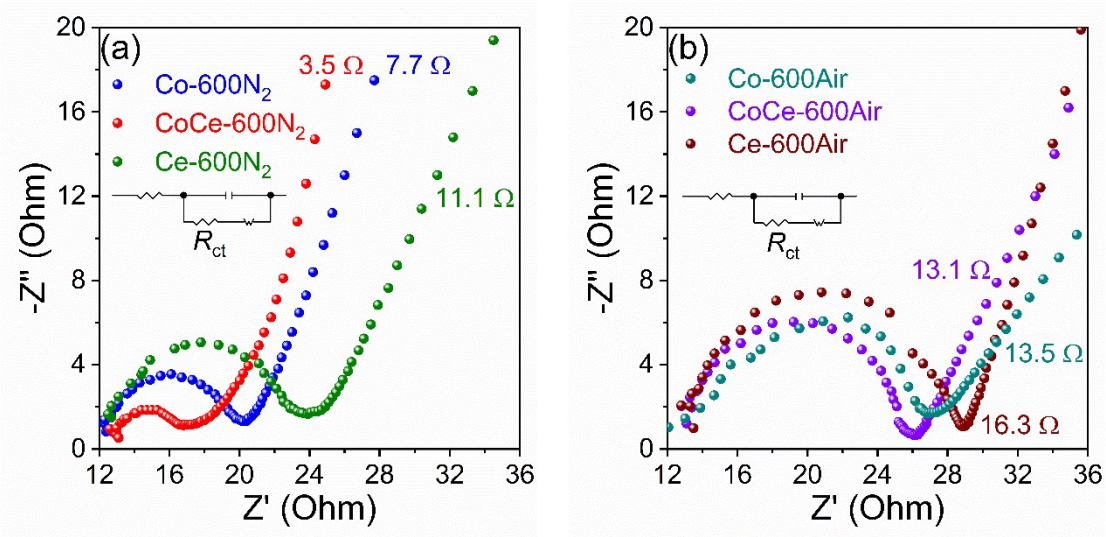

Fig. S8. EIS Nyquist plots at the open circuit potential and the simulated equivalent circuit (inset) for (a) Co-600N_2, Ce-600N_2, CeCo-600N_2 and (b) Co-600Air, Ce-600Air, CeCo-600Air.

\

Supplementary Tables

Table S1. Pore structures for the electrocatalysts prepared in N_2 and air.

Samples	BET SSA (m^2 g^{-1})	Pore volume (cm^3 g^{-1})	Micropore size (nm)	Mesopore size (nm)
Co-600N_2	165.4	0.29	0.41	2.39
CoCe-600N_2	173.5	0.22	0.50	2.23
Ce-600N_2	287.1	0.36	0.45	2.56
Co-600Air	15.1	0.03	--	2.05
CoCe-600Air	31.5	0.07	--	2.04
Ce-600Air	54.8	0.18	--	2.22

Table S2. Binding energy of different species determined by XPS.

Samples	N 1s				Ce 3d $_{5/2}$		Co 2p $_{3/2}$			O 1s		
	Pyridinic -N	Pyrrolic -N	Quaternary -N	Oxidized -N	Ce^{3+}	Ce^{4+}	Co^{0}	Co^{2+}	Co^{3+}	O3	O2	O1
Co-600N_2	398.5	399.8	400.9	--	--	--	778.1	781.6	779.7	530.0	531.7	533.6
CoCe-600 N_2	398.4	399.6	400.9	406.4	884.6, 903.1	882.3, 888.7,898.2, 900.8, 907.7,916.7	--	781.1	779.5	529.8	531.5	532.9
Ce-600 N_2	398.2	399.7	400.8	406.7	884.2, 902.9	882.1, 888.4,	--	--	--	529.7	531.4	532.8

						897.9, 900.6, 907.5, 916.5						
Co-600Air	--	--	--	--	--	--	--	781.1	779.7	530.2	531.6	533.1
CoCe-600Air	--	--	--	--	884.8, 902.9	882.4, 889.2, 898.4, 900.9, 907.8, 916.8	--	780.9	779.5	529.8	531.4	532.3
Ce-600Air	--	--	--	--	884.9, 903.0	882.3, 889.0, 898.3 990.8,	--	--	--	529.6	530.8	532.0

907.8, 916.7

Table S3. The surface compositions of the samples determined by XPS.

Samples	N 1s (at. %)					Ce 3d (at. %)				Co 2p (at. %)				O 1s (at. %)			
	Pyridinic-N	Pyrrolic-N	Quaternary-N	Oxidized-N	Total N	Ce^{3+}/	Ce^{4+}	Total Ce	Co^{0}	Co^{2+}	Co^{3+}	Co^{2+}+Co^{3+}	Total Co	O3	O2	O1	Total O
Co-600N_2	1.78	1.54	1.51	--	4.83	--	--	--	0.53	0.93	1.03	1.96	2.49	1.02	3.42	1.21	5.65
CoCe-600N_2	1.79	1.63	2.07	2.10	7.59	0.42	1.64	2.06	--	5.88	5.72	11.6	11.6	19.79	9.16	5.06	34.01
Ce-600N_2	0.98	1.71	1.37	0.64	4.7	0.89	4.62	5.51	--	--	--	--	--	16.03	7.90	3.53	27.46
Co-600Air	--	--	--	--	--	--	--		--	5.72	5.25	10.97	10.97	20.63	5.37	4.95	30.95

CoCe-600Air	--	--	--	--	--	1.18	4.23	5.41	--	7.72	5.26	12.98	12.98	31.52	6.22	3.11	40.85
Ce-600Air	--	--	--	--	--	2.46	11.53	13.99	--	--	--	--	--	33.63	4.58	3.90	42.11

Table S4. Summary of ORR and OER activity of the samples prepared in air.

Electrocatalysts	ORR activity					OER activity				Overall evaluation
	Onset Potential (V)	Half-wave potential (V)	Limiting current Density (mA cm^{-2})	Current density at 0.76 (mA cm^{-2})	ORR Tafel Slope (mV dec^{-1})	Potential @ 10 mA cm^{-2} $E_{j=10}$ (V)	Overpotential@ 10 mA cm^{-2} η_{10} (mV)	Current density at overpotential of 470 mV (V)	OER Tafel Slope (mV dec^{-1})	$\Delta E = E_{j=10} - E_{1/2}$ (V)
Co-600Air	0.90	0.68	3.94	0.15	79.0	1.741	511	4.67	105.3	1.06
CoCe-600Air	0.92	0.74	4.44	0.29	68.6	1.657	427	16.42	99.2	0.92
Ce-600Air	0.75	0.61	2.82	0.01	88.9	N.A	N.A	0.52	387.7	N.A

Table S5. Comparison of the bifunctional activity of the recently reported oxygen electrocatalysts.

Electrocatalyst	Electrolyte	$E_{1/2}$ (V) vs. RHE	$E_{j=10}$ (V) vs. RHE	ΔE (V) ($E_{j=10}$-$E_{1/2}$)	Refs.
CeO_2/Co_3O_4@NC	0.1 M KOH	0.87	1.51	0.64	This work
Co-N@HCS	0.1 M KOH	0.86	1.72	0.86	S1
3D NCNT array	0.1 M KOH	0.81	1.65	0.84	S2
Pd@PdO-Co_3O_4	0.1 M KOH	0.73	1.54	0.81	S3
RuO_2	0.1 M KOH	0.37	1.64	1.27	S4
Pt/C	0.1 M KOH	0.90	1.90	1.00	S4
Co@Co_3O_4/NC-1	0.1 M KOH	0.80	1.65	0.85	S4
CoO/N-graphene	1 M KOH	0.81	1.57	0.76	S5
NC@Co-NGC DSNCs	0.1 M KOH	0.82	1.64	0.82	S6
Co-CoO-Co_3O_4/NC	0.1 M KOH	0.80	1.63	0.83	S7

Table S6. ORR and OER mass activity of the resulting electrocatalysts prepared in air.

Electrocatalysts	ORR mass activity (A g_{cat}^{-1}) [a)]	OER mass activity (A g_{cat}^{-1}) [b)]
Co-600Air	0.63	19.46
CoCe-600Air	1.21	68.42
Ce-600Air	0.04	2.17

[a)] The ORR mass activity was obtained through normalization of kinetic current density at 0.76 V to the mass loading of the resulting electrocatalysts on the GC electrode. [b)] The OER mass activity was obtained by normalization of current density at the overpotential of 470 mV to the loading mass of the resulting electrocatalysts on the GC electrode.

Table S7. Comparisons of the performance of Zn-air batteries with recently reported bifunctional electrocatalysts.

Electrocatalyst	Electrolyte	Specific capacity (mAh g_{Zn}^{-1})	Energy density (Wh kg_{Zn}^{-1})	Cycle Condition (mA cm^{-2})	Refs.
CeO_2/Co_3O_4@NC	6.0 M KOH + 0.10 M $ZnCl_2$	643	805	5	This work
NGM-Co	6.0 M KOH + 0.20 M $ZnCl_2$	750	840	2	S8
NPMC-1000	6.0 M KOH	735	835	2	S9
CoNi@NCNT/NF	6.0 M KOH + 0.20 M $Zn(Ac)_2$	655	845	5	S10
Co@Co_3O_4@NC-900	6.0 M KOH	640	--	5	S11
Mo–N/C@MoS_2	6.0 M KOH + 0.20 M $Zn(Ac)_2$	--	846.07	5	S12
CNT/graphene	6.0 M KOH	712	872	5	S13
Porous C fiber film	6.0 M KOH + 0.20 M $Zn(Ac)_2$	660	838	5	S14
Co_3O_4/N-rGO	6.0 M KOH + 0.20 M $ZnCl_2$	550	649	6	S15

NCNF/$Co_xMn_{1-x}O$	6.0 M KOH + 0.20 M $ZnCl_2$	581	695	7	S16
NCNT/CoO-NiONiCo	6.0 M KOH + 0.20 M $ZnCl_2$	594	713	7	S17
NCNF/$Co_xMn_{1-x}O$	6.0 M KOH + 0.20 M $ZnCl_2$	581	695	7	S16
NCNT/CoO-NiONiCo	6.0 M KOH + 0.20 M $ZnCl_2$	594	713	7	S17
NCNF	6.0 M KOH + 0.20 M $ZnCl_2$	626	776	10	S14
Porous C fiber film	6.0 M KOH + 0.20 M $Zn(Ac)_2$	626	776	10	S14
CoZn-NC-700	6.0 M KOH + 0.10 M $ZnCl_2$	578	694	10	S18
Ni_3Fe/N-C	6.0 M KOH + 0.20 M $ZnCl_2$	528	634	10	S19
$NiCo_2S_4$/N-CNT	6.0 M KOH + 0.20 M $ZnCl_2$	431.1	554.6	10	S20
BHPC-950	6.0 M KOH	797	963	20	S21
NCO-A1	6.0 M KOH	580	--	20	S22
Ag-Cu on Ni foam	6.0 M KOH + 0.20 M $ZnCl_2$	572	641	20	S23

CoO/N-CNT+NiFe LDH	6.0 M KOH + 0.20 M $ZnCl_2$	570	700	20	S24
CoO NRs	6.0 M KOH	541.3	583.3	20	S25
NCNT/CoO-NiONiCo	6.0 M KOH + 0.20 M $ZnCl_2$	545	615	20	S17

Supplementary References

S1. S. C. Cai, Z. H. Meng, H. L. Tang, Y. Wang and P. Tsiakaras, *Appl. Catal., B*, 2017, **217**, 477-484.

S2. Z. H. Li, M. F. Shao, Q. H. Yang, Y. Tang, M. Wei, D. G. Evans and X. Duan, *Nano Energy*, 2017, **37**, 98-107.

S3. H. C. Li, Y. J. Zhang, X. Hu, W. J. Liu, J. J. Chen and H. Q. Yu, *Adv. Energy Mater.*, 2018, **8**, 1702734.

S4. A. Aijaz, J. Masa, C. Rösler, W. Xia, P. Weide, A. J. Botz, R. A. Fischer, W. Schuhmann and M. Muhler, *Angew. Chem. Int. Ed.*, 2016, **55**, 4087-4091.

S5. S. Mao, Z. Wen, T. Huang, Y. Hou and J. Chen, *Energy Environ. Sci.*, 2014, **7**, 609-616.

S6. S. Liu, Z. Wang, S. Zhou, F. Yu, M. Yu, C. Y. Chiang, W. Zhou, J. Zhao and J. Qiu, *Adv. Mater.*, 2017, **29**, 1700874.

S7. X. R. Yi, X. B. He, F. X. Yin, B. H. Chen, G. R. Li and H. Q. Yin, *Electrochim. Acta*, 2019, **295**, 966-977.

S8. C. Tang, B. Wang, H. F. Wang and Q. Zhang, *Adv. Mater.*, 2017, **29**, 1703185.

S9. J. Zhang, Z. Zhao, Z. Xia and L. Dai, *Nat. Nanotechnol.*, 2015, **10**, 444-452.

S10. W. Niu, S. Pakhira, K. Marcus, Z. Li, J. L. Mendoza-Cortes and Y. Yang, *Adv. Energy Mater.*, 2018, **8**, 1800480.

S11. Z. Guo, F. Wang, Y. Xia, J. Li, A. G. Tamirat, Y. Liu, L. Wang, Y. Wang and Y. Xia, *J. Mater. Chem. A*, 2018, **6**, 1443-1453.

S12. I. S. Amiinu, Z. Pu, X. Liu, K. A. Owusu, H. G. R. Monestel, F. O. Boakye, H.

Zhang and S. Mu, *Adv. Funct. Mater.*, 2017, **27**, 1702300.

S13. J. Yang, H. Sun, H. Liang, H. Ji, L. Song, C. Gao and H. Xu, *Adv. Mater.*, 2016, **28**, 4606-4613.

S14. Q. Liu, Y. Wang, L. Dai and J. Yao, *Adv. Mater.*, 2016, **28**, 3000-3006.

S15. Y. Li, C. Zhong, J. Liu, X. Zeng, S. Qu, X. Han, Y. Deng, W. Hu and J. Lu, *Adv. Mater.*, 2018, **30**, 1703657.

S16. X. Liu, M. Park, M. G. Kim, S. Gupta, X. Wang, G. Wu and J. Cho, *Nano Energy*, 2016, **20**, 315-325.

S17. X. Liu, M. Park, M. G. Kim, S. Gupta, G. Wu and J. Cho, *Angew. Chem. Int. Ed.*, 2015, **54**, 9654-9658.

S18. B. Chen, X. He, F. Yin, H. Wang, D.-J. Liu, R. Shi, J. Chen and H. Yin, *Adv. Funct. Mater.*, 2017, **27**, 1700795.

S19. G. Fu, Z. Cui, Y. Chen, Y. Li, Y. Tang and J. B. Goodenough, *Adv. Energy Mater.*, 2017, **7**, 1601172.

S20. X. Han, X. Wu, C. Zhong, Y. Deng, N. Zhao and W. Hu, *Nano Energy*, 2017, **31**, 541-550.

S21. M. Yang, X. Hu, Z. Fang, L. Sun, Z. Yuan, S. Wang, W. Hong, X. Chen and D. Yu, *Adv. Funct. Mater.*, 2017, **27**, 1701971.

S22. M. Prabu, K. Ketpang and S. Shanmugam, *Nanoscale*, 2014, **6**, 3173-3181.

S23. Y. Jin and F. Chen, *Electrochim. Acta*, 2015, **158**, 437-445.

S24. Y. Li, M. Gong, Y. Liang, J. Feng, J. E. Kim, H. Wang, G. Hong, B. Zhang and H. Dai, *Nat. Commun.*, 2013, **4**, 1805.

S25. P. Da, M. Wu, K. Qiu, D. Yan, Y. Li, J. Mao, C. Dong, T. Ling and S. Qiao, *Chem. Eng. Sci.*, 2019, **194**, 127-133.